
Personalized Neural Architecture Search for Federated Learning

Minh Hoang

Department of Computer Science
Carnegie-Mellon University
Pittsburgh, PA 15213
qhoang@andrew.cmu.edu

Carl Kingsford

Computational Biology Department
Carnegie Mellon University
Pittsburgh, PA 15213
carlk@cs.cmu.edu

Abstract

Federated Learning (FL) is a recently proposed learning paradigm for decentralized devices to collaboratively train a predictive model without exchanging private data. Existing FL frameworks, however, assume a one-size-fit-all model architecture to be collectively trained by local devices, which is determined prior to observing their data. Even with good engineering acumen, this often falls apart when local tasks are different and require diverging choices of architecture modelling to learn effectively. This motivates us to develop a novel personalized neural architecture search (NAS) algorithm for FL, which learns a base architecture that can be structurally personalized for quick adaptation to each local task. On several real-world datasets, our algorithm, FEDPNAS is able to achieve superior performance compared to other benchmarks on heterogeneous multitask scenarios.

1 Introduction

Federated Learning (FL) [McMahan et al., 2017, Vo et al., 2021, Li et al., 2020] is a variant of distributed learning [Hoang et al., 2019a,b] where the objective function \mathcal{L} can be decomposed into a linear combination of M local objective functions $\{\mathcal{L}_i\}_{i=1..M}$. Each function depends on its local private data and a set of shared parameters w . Specifically, let \mathcal{D}_i denote the i^{th} local training dataset, ψ denote the w -parameterized neural network architecture chosen for the federated task, and $\ell(x, y)$ denote the loss incurred by predicting $\psi(x; w)$ with ground truth y , we define the FL objective as:

$$\operatorname{argmin}_w \mathcal{L}(w) = \operatorname{argmin}_w \sum_{i=1}^M \mathcal{L}_i(w | \mathcal{D}_i) \triangleq \operatorname{argmin}_w \mathbb{E}_{(x,y) \sim \mathcal{D}_i} [\ell(x, y; \psi)]. \quad (1)$$

This is not applicable to scenarios where local models are expected to solve different tasks which are similar in broad sense yet diverge in finer details [Lam et al., 2021, Hoang et al., 2020, Yurochkin et al., 2019]. For example, consider the task of recognizing the outcome of a coin flip given images collected by two clients: one capture the coin from above, the other from below. This setting implies that when the same input image is provided by both clients, the correct classifications must be the opposite of one another. However, since existing FL methods converge on a single model architecture and weight, there can only be one predictive outcome which cannot satisfy both tasks.

To relax this constraint, the recent work of Fallah et al. [2020] extends FL by incorporating ideas from meta learning [Finn et al., 2017] which results in a new framework of personalized FL. The new framework can accommodate for such task heterogeneity but still requires all client models to agree on a single architecture beforehand, which is sub-optimal. To address this shortcoming, one naive idea is to adopt existing ideas in Neural Architecture Search (NAS) via Reinforcement Learning [Zoph and Le, 2016, Pham et al., 2018] which act as an outer loop to the existing FL routine.

However, this simple approach does not allow client models to adapt to local tasks on an architecture level and is often not preferred due to the cost of repeated FL training. This paper proposes a novel personalized NAS algorithm for federated learning, which generalizes ideas in respective areas of NAS [Zoph and Le, 2016, Pham et al., 2018] originally developed for single-task scenarios, and FL [Fallah et al., 2020] under a unified len of federated personalized neural architecture search (FEDPNAS).

In particular, to customize the model architecture for each task in the FL workflow, FEDPNAS first represents the model architecture for each task as a sub-network sampled from a large, over-parameterized network. The sampling distribution is (collaboratively) learned along with the parameters of the sampled network via a generalization of the recently proposed Discrete Stochastic NAS (DSNAS) method [Hu et al., 2020]. Unlike DSNAS, which lacks the ability to customize architecture for individual tasks, our generalized FEDPNAS incorporates model personalization on an architecture level. Our contributions include:

1. A novel architecture that factorizes into a base component (shared across tasks) and a personalizable component, which respectively capture the task-agnostic and task-specific information (Section 3.1).
2. A context-aware sampling distribution conditioned on specific task instance, which captures task-specific information and naturally incorporates personalization into architecture search (Section 3.3).
3. An FL algorithm that optimizes for a common architecture, followed by a personalization phase where each client subsequently adapts only the *personalized component* to fit its own task via fine-tuning with local data. To ensure that the common architecture distribution converges at a *vantage* point that is relevant and beneficial to all clients, we generalize the vanilla FL objective in Eq. (1) such that local gradient steps directly optimize for expected improvement resulting from future fine-tuning (Section 3.2).

2 Related Work

Two-stage Neural Architecture Search: Most existing NAS frameworks separately optimize for the optimal architecture and its parameters in two stages: *searching* and *evaluation*. The former stage usually employs evolutionary-based strategies [Floreano et al., 2008, Real et al., 2019], Bayesian optimization surrogates [Bergstra et al., 2013, Hu et al., 2018] or Reinforcement Learning controllers [Baker et al., 2016, Zoph and Le, 2016, Pham et al., 2018] to propose candidate architectures based on random mutations and/or observed experience; while the latter optimizes the parameters of these architectures given task data and provide feedback to improve the search agent.

Naturally, an extension of such methods to the FL setting is through distributing the evaluation workload over many clients, which does not require exposing private data. A pioneering work in this direction is FEDNAS [He et al., 2020]. In practice, however, two-stage federated NAS frameworks are generally not suitable for the personalized FL setting for two reasons: (a) the clients often lack the computational capacity to repeatedly optimize the parameters for many candidate architectures; and (b) the clients have to converge on a single architecture proposed by the central search agent.

Discrete Stochastic Neural Architecture Search: Discrete stochastic neural architecture search (DSNAS) [Hu et al., 2020] addresses the computational issue of two-stage NAS by jointly optimizing the optimal architecture and its weight in an end-to-end fashion, which allows users to continually train a single network on demand over time as opposed to performing full parameter optimization for every candidate until a good architecture is discovered.

The main idea of DSNAS is to combine weight training for an over-parameterized master architecture with discrete computational path sampling. DSNAS parameterizes the master architecture as a stack of modular cells: $\psi(x) = \psi_C \circ \psi_{C-1} \cdots \circ \psi_1(x)$ ¹, where x is an arbitrary input, C is the number of cells, ψ_t denotes the t^{th} cell in the stack, and \circ denotes the compositional operator. The inner computation of ψ_t is in turn characterized by a directed acyclic graph (DAG) with V nodes $\{v_i\}_{i=1}^{|V|}$, where each node represents some intermediate feature map. For each directed edge (v_i, v_j) , there is an associated list of D possible network operations $\mathbf{O}_{ij} = [o_{ij}^1, o_{ij}^2 \dots o_{ij}^D]$ ² where each operation o_{ij}^k transforms v_i to v_j . Here, v_1 corresponds to the output of previous cell ψ_{t-1} (or

¹In this description, we assume each DSNAS cell receives input from only one previous cell.

²We drop the cell index in the definition operation for ease of notation.

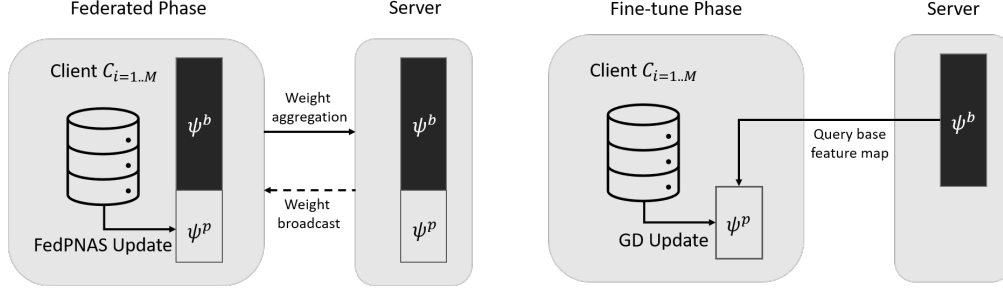


Figure 1: Our proposed method FEDPNAS. FL phase: each client updates both base (ψ^b) and personalized components (ψ^p) (Section 3.2); then sends its parameters to the server for aggregation. Fine-tune phase: each client continues to update only the personalized component.

input x when $t = 1$). We recursively define intermediate nodes $v_j = \sum_{i=1}^{j-1} \mathbf{Z}_{ij}^\top \mathbf{O}_{ij}(v_i)$, where $\mathbf{O}_{ij}(v_i) \triangleq [o_{ij}^1(v_i), o_{ij}^2(v_i) \dots o_{ij}^D(v_i)]$ and \mathbf{Z}_{ij} is a one-hot vector sampled from the categorical distribution $p(\mathbf{Z} \mid \mathbf{\Pi})$ where the event probabilities $\mathbf{\Pi} = \{\pi_1, \pi_2, \dots, \pi_D \mid \sum_{i=1}^D \pi_i = 1\}$ are learnable. Essentially, learning the distribution $p(\mathbf{Z})$ allows us to sample computational paths or sub-graphs of the original DAG that correspond to high-performing, compact architecture from the over-parameterized master network. Sampling discrete random variables from $p(\mathbf{Z})$, however, does not result in a gradient amenable to back-propagation. To sidestep this issue, DSNAS adopts the *straight-through* Gumbel-softmax trick [Jang et al., 2016], which re-parameterizes the k^{th} index of the one-hot variable as $\mathbf{Z}_{ij}[k] = \mathbb{I}\left(k \triangleq \arg \max_t [g_t + \log \pi_t]\right)$, where $g_t \sim \text{Gumbel}(0, 1)$. While this *forward* computation does not have a gradient by itself, we can estimate the gradient through a proxy during the *backward* pass:

$$\nabla \mathbf{Z}_{ij}[k] \simeq \nabla \tilde{\mathbf{Z}}_{ij}[k] \triangleq \nabla \left(\frac{\exp((g_k + \log \pi_k) / \tau)}{\sum_{t=1}^D \exp((g_t + \log \pi_t) / \tau)} \right) \quad (2)$$

which is unbiased when converged as the temperature τ is steadily annealed to 0 [Jang et al., 2016]. This formulation, however, is not easily extended to the FL setting, especially when local tasks are not homogeneous. We describe the key challenges in Section 3, together with our proposed approaches.

3 Personalized NAS for Federated Learning

Let \mathbf{W} denote the concatenated weights of all network operations in the network architecture. The set up above of DSNAS [Jang et al., 2016] is naively extendable to a FL setting:

$$\operatorname{argmin}_{\mathbf{W}, \mathbf{\Pi}} \mathcal{L}(\mathbf{W}, \mathbf{\Pi}) \equiv \operatorname{argmin}_{\mathbf{W}, \mathbf{\Pi}} \frac{1}{M} \sum_{i=1}^M \mathcal{L}_i(\mathbf{W}, \mathbf{\Pi} \mid \mathcal{D}_i). \quad (3)$$

McMahan et al. [2017] optimizes this objective by alternating between (a) central agent broadcasting aggregated weights to local clients and (b) local clients sending gradient descent updated weights (given local data) to the central agent for aggregation. This, however, implies that after the last central aggregation step, all clients will follow the same architecture distribution induced by the final broadcasted copy of \mathbf{W} and $\mathbf{\Pi}$. As previously argued, this is not optimal in a heterogenous task setting which requires task-specific adaptation for local clients to achieve good performance.

Furthermore, having the same sampling distribution $p(\mathbf{Z})$ regardless of context (i.e., feature maps received as cell input) limits the architecture discovery to those that perform reasonably on average over the entire dataset. However, we remark that restricting the architecture to be the same for every input samples is unnecessary and undermines the expressiveness of an over-parameterized search space. On the other hand, letting the architecture be determined on a *per-sample* basis makes better use of the search space and potentially improves the predictive performance.

The focus of this work is therefore to incorporate both task-wise and context-wise personalization to federated neural architecture search in multitask scenarios, which is achieved through our proposed

algorithm FEDPNAS. In general, FEDPNAS functions similarly to the vanilla FEDDSNAS algorithm described above, with an addition of a fine-tuning phase at each local client after the FL phase to adapt the aggregated common model for local task data, as shown in Fig. 1. To make this work, however, we need to address the following **key challenges**:

C1. First, as previously argued in Section 1, tasks across federated clients tend to share similarities in broad sense, and diverge in finer details. A good federated personalization search space, therefore, need to capture this fundamental observation through design and appropriate resource distribution. We address this challenge in Section 3.1.

C2. Second, an over-parameterized architecture search space offers the flexibility of having specific computation paths for different samples. This is not exploited by DSNAS as reflected in its choice of context-independent sampling distribution $p(\mathbf{Z})$. To address this, Section 3.3 proposes a novel parameterization of $p(\mathbf{Z})$ to incorporate context information into operator sampling.

C3. Last, the common model may not be universally useful to all local clients, which makes it difficult to be fine-tuned. To address this concern, Section 3.2 proposes a new personalized federated NAS objective inspired by Finn et al. [2017] to optimize the common model in anticipation of further fine-tuning by the client models.

3.1 Personalizable Architecture Search Space

Similar to DSNAS [Hu et al., 2020], we adopt a cell-based representation to trade-off search space expressiveness for efficiency. Unlike the original design, which assumes similar role for every cell in the architecture stack (i.e., implied by the fully factorizable path sampling distribution $p(\mathbf{Z})$), we split our cells into two component stacks with separate meta-roles catering to the federated personalization task: (a) a *base stack* $\psi_b = \{\psi_1^b, \psi_2^b \dots \psi_{C_b}^b\}$ which aims to capture the broad commonalities of data samples across client tasks; and (b) *personalized stack* $\psi_p = \{\psi_1^p, \psi_2^p \dots \psi_{C_p}^p\}$, which will be fine-tuned with local data to capture task-specific details.

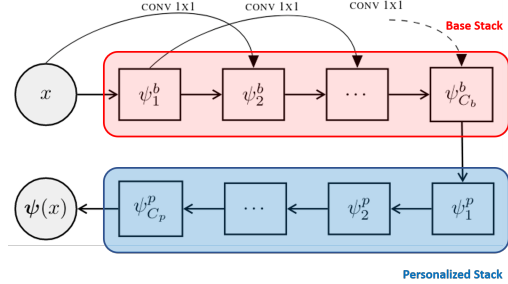


Figure 2: Feature mapping down the component stacks of our architecture space. Base cells receive outputs from two previous cells. Personalized cells receive outputs from only one previous cell.

We explain the main difference between these components to account for different level of expressiveness requirements below:

Base stack. Every cell ψ_t^b in the base stack takes as inputs the outputs of its previous two cells ψ_{t-1}^b and ψ_{t-2}^b (replaced with raw input x when necessary for $t \leq 2$). The output of the skip-ahead cell ψ_{t-2}^b is additionally passed through a 1×1 convolution layer as a cost-effective way to control the number of channels. Additionally, the operators available to the base cell include large convolution layers with size 5×5 and 7×7 . To compensate for the growing number of channels, we periodically employ a reduction convolution (with stride larger than 1) similar to DSNAS [Hu et al., 2020] to reduce the feature dimension down the stack.

Personalized stack. As opposed to the design of the base cells above, every cell ψ_t^p in the personalized stack has minimal expressiveness. That is, ψ_t^p excludes large operators and only takes as input the output of its immediate predecessor ψ_{t-1}^p (or $\psi_{C_b}^b$ when $t = 1$). There are two reasons for this choice. First, as the fine-tuning phase has access to fewer data samples than the federated phase, having a more compact fine-tuning space helps to improve the rate of convergence. Second, as we will discuss in Section 3.3 below, our personalized FL objective requires the Hessian of the personalized parameters, which is computationally expensive. As such, we only restrict the personalization to happen on the more compact personalized stack.

3.2 Personalized Federated Learning Objective

Unlike FEDAVERAGING [McMahan et al., 2017], which assumes the clients will follow the consensus base model obtained after the federated phase, FEDPNAS expects clients to further personalize

the base model with local task data. That said, while the base model is trained to work well in the expected sense over the task distribution, there is no guarantee that it is a good initial point for every client model to improve upon via fine-tuning. To address this, we adopt the concept of training in anticipation of future adaptation introduced by MAML [Finn et al., 2017]. That is, during client update, instead of optimizing the loss with respect to the same consensus weight, each client will instead optimize the weight perturbed by a small gradient step in the fine-tuning direction.

For simplicity, let $\theta = \{\theta_b, \theta_p\}$ respectively denote all trainable parameters of the base stack and the personalized stack, i.e., $\theta_b = \{\mathbf{W}_b, \mathbf{\Pi}_b\}$, $\theta_p = \{\mathbf{W}_p, \mathbf{\Pi}_p\}$. The personalized FL objective at client i is then given by $\tilde{\mathcal{L}}_i(\theta_b, \theta_p) \triangleq \mathcal{L}_i(\theta_b, \tilde{\theta}_p)$ where $\tilde{\theta}_p \triangleq \theta_p - \eta \nabla_{\theta_p} \mathcal{L}_i(\theta_b, \theta_p)$ adjusts the parameters of the personalized component to account for a small fine-tuning gradient step. The adjusted local loss only depends on the respective client data and is amenable to federated learning. The local update gradient, however, involves a Hessian term whose computation is expensive to repeat over many epochs. To circumvent this problem, we use the first-order Taylor approximation to estimate the Hessian term by the outer product of Jacobian, which results in a gradient that requires exactly two forward/backward passes to compute:

$$\nabla_{\theta_p} \tilde{\mathcal{L}}_i = \left(\mathbf{I} - \eta \nabla_{\theta_p}^2 \mathcal{L}_i \right) \left(\nabla_{\tilde{\theta}_p} \tilde{\mathcal{L}}_i \right) \simeq \left(\mathbf{I} - \eta \nabla_{\theta_p}^\top \mathcal{L}_i \nabla_{\theta_p} \mathcal{L}_i \right) \left(\nabla_{\tilde{\theta}_p} \tilde{\mathcal{L}}_i \right),$$

where \mathcal{L}_i and $\tilde{\mathcal{L}}_i$ are short-hands for $\mathcal{L}_i(\theta_b, \theta_p)$ and $\tilde{\mathcal{L}}_i(\theta_b, \theta_p)$ respectively. The FL phase of our FEDPNAS framework is detailed in Alg. 1 (Appendix A). An instance of FEDPNAS’s forward and backward pass which sequentially unrolls down the component stacks, alternating between sampling and evaluation, is in turn given in Alg. 2 (Appendix A).

3.3 Context-aware Operator Sampler

The choice of a fully factorizable sampling distribution $p(\mathbf{Z})$ in DSNAS follows that of SNAS [Xie et al., 2018], which argues that the Markov assumption for $p(\mathbf{Z})$ is not necessary because NAS has fully delayed rewards in a deterministic environment. However, this generally only holds for two-stage NAS (Section 2) and does not apply to end-to-end frameworks such as SNAS and DSNAS. We instead take advantage of the over-parameterized architecture via factorizing the conditional $p(\mathbf{Z} | x)$, which takes into account the temporal dependency of structural decisions:

$$p(\mathbf{Z} | x) \simeq p(\mathbf{Z}_1 | x) \prod_{t=2}^C p(\mathbf{Z}_t | v_1^t, x) = p(\mathbf{Z}_1 | x) \prod_{t=2}^C \prod_{(i,j)} p(\mathbf{Z}_{ij}^t | v_1^t, x), \quad (4)$$

where \mathbf{Z}_t , \mathbf{Z}_{ij}^t and v_1^t respectively denote all the samples, the sample at edge (i, j) and the input at cell ψ_t . We have also assumed a single stack setting since the parameterization of $p(\mathbf{Z})$ does not differ between base and personalized cells.

To reduce computational complexity, instead of conditioning the samples of subsequent cells on previous \mathbf{Z} samples, we approximate $p(\mathbf{Z}_t | \mathbf{Z}_{t-1} \dots \mathbf{Z}_1, x) \simeq p(\mathbf{Z}_t | v_1^t, x)$ by the assumption that the cell contents are conditionally independent given the immediate cell input and the original input. Finally, we assume that $p(\mathbf{Z}_t | v_1^t, x)$ is fully factorizable across edges in the same cell and parameterize $p(\mathbf{Z}_{ij}^t | v_1^t, x) = \phi^{(i,j)}(v_1^t, x)$ where ϕ is a deep classification network whose output dimension equal the number of edges in cell ψ_t . Samples of \mathbf{Z}_{ij}^t can then be generated using the straight-through Gumbel-softmax reparameterization similar to Jang et al. [2016].

4 Experiments

This section describes our experiments to showcase the performance of FEDPNAS compared to different NAS and FL benchmarks on various scenarios. All of our empirical studies are conducted on two image recognition datasets: (a) the CIFAR-10 dataset [Krizhevsky et al., 2009] which aims to predict image labels from 10 classes given a train/test set of 50000/10000 colour images of dimension 32×32 pixels; and (b) the MNIST dataset [LeCun et al., 2010] which aims to predict handwritten digits (i.e. 0 to 9) given a train/test set of 60000/10000 grayscale images of dimension 28×28 pixels. Our search space entails 2^{40} possible architectures, which is detailed in Appendix D. We compare two variants of our framework, CA-FEDPNAS (with context-aware operation sampler) and FEDPNAS (without the operation sampler), against: (a) FEDAVERAGING of a fixed architecture to

justify the need for NAS in FL; (b) FEDDSNAS: the federated extension of DSNAS (Section 3), to show the effectiveness of our proposed context-aware sampler on NAS performance; and finally (c) CA-FEDDSNAS, which extends FEDDSNAS with our context-aware sampler.

On simulate heterogenous predictive tasks. To simulate this scenario, we first distribute the data i.i.d across clients (10000/2000 and 12000/2000 training/test images per client for CIFAR-10 and MNIST datasets respectively). Then, we independently apply a different transformation to each partitioned dataset. Input images within the same train/test set is subject to the same transformation. In both our experiments, the client datasets are subjected to rotations of -30° , -15° , 0° , 15° and 30° respectively. This data generation protocol reflects a realistic and frequently seen scenario where independently collected data of the same phenomenon might contain systematic bias due to measurement errors and/or different collection protocols. Fig. 3 below shows the performance of all the methods in comparison, plotted against number of search epochs and averaged over the above rotated variants of CIFAR-10 and MNIST datasets.

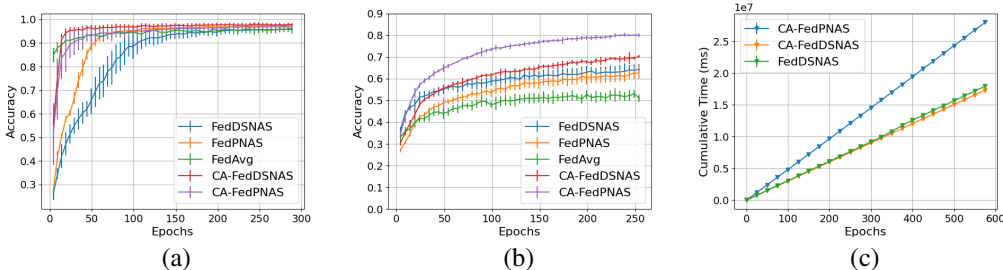


Figure 3: Plotting average classification accuracy of various methods against no. training epochs on heterogeneous tasks derived from (a) MNIST dataset; and (b) CIFAR-10 dataset. Figure (c) compares cumulative running time of various methods against no. training epochs on CIFAR-10 dataset.

On the MNIST dataset (Fig. 3b), all methods eventually converge to a similar performance. Among the NAS benchmarks, FEDPNAS and FEDDSNAS both converge slower than FEDAVG and start off with worse performance in early iterations, which is expected since FEDAVG does not have to search for the architecture and it is likely that the default architecture is sufficient for the MNIST task. On the other hand, we observe that both CA-FEDPNAS and CA-FEDDSNAS converge much faster than their counterparts without the context-aware operation sampler component. This shows that making use of contextual information helps to quickly locate regions of high-performing architectures, especially on similar inputs.

On the CIFAR-10 dataset (Fig. 3a), we instead observe significant gaps between the worst performing FEDAVG and other NAS methods. This is likely because the default architecture does not have sufficient learning capability, which confirms the need for customizing solutions. Among the NAS benchmarks, we again observe that both CA-FEDPNAS and CA-FEDDSNAS outperform their counterparts without our operation sampler, which confirms the intuition above. Most remarkably, our proposed framework CA-FEDPNAS achieves the best performance (0.8) and significantly outperformed both variants of federated DSNAS (0.71 for CA-FEDDSNAS and 0.63 for FEDDSNAS).

Lastly, Fig. 3c shows the runtime comparison between three methods on the CIFAR-10 experiment. In terms of sampling time, we observe that there is negligible overhead incurred by using our context-aware sampler (CA-FEDDSNAS vs. FEDDSNAS). The time incurred by our update (CA-FEDPNAS) scales by a constant factor compared to CA-FEDDSNAS since we use exactly one extra forward/backward pass per update.

On objectives with varying heterogeneity. We expand the above study by investigating respective performance of CA-FEDPNAS and FEDDSNAS on tasks with varying levels of heterogeneity. At low level of heterogeneity, we deploy these methods on 5 sets of slightly rotated MNIST images. At high level of heterogeneity, we employ a more diverse set of transformations on MNIST images, such as hue jitter and large angle rotations of 90° and -90° . Table 1 show the respective result of each task from these two settings. We observe that our method CA-FEDPNAS achieves better performance on most tasks and the performance gaps on tasks with higher heterogeneity are more pronounced (i.e., up to 7% improvement on ROTATE 90 task). This clearly shows the importance of architecture personalization when the training tasks are significantly different and justifies our research goal.

HETEROGENEITY	TASK DESCRIPTION	FEDDSNAS	CA-FEDPNAS
LOW	ROTATE -30	0.947	0.978
	ROTATE -15	0.973	0.976
	VANILLA	0.988	0.985
	ROTATE 15	0.986	0.987
	ROTATE 30	0.972	0.981
HIGH	HUEJITTER -0.5	0.966	0.978
	HUEJITTER 0.5	0.967	0.972
	VANILLA	0.988	0.989
	ROTATE -90	0.892	0.932
	ROTATE 90	0.866	0.932

Table 1: Predictive accuracy of CA-FEDPNAS vs. FEDDSNAS on tasks with varying heterogeneity levels. ROTATE X denotes a rotation transformation of X° on client data; VANILLA denotes the original MNIST images; and HUEJITTER X denotes a hue jitter transformation of training images by a factor of X. The best performance in each row is in bold font.

On knowledge transfer to completely new tasks. Finally, we investigate a scenario where the architecture distributions discovered by CA-FEDPNAS and FEDDSNAS are required to generalize to completely unseen tasks. Particularly, we train both methods on five clients whose local data consist of 12000 slightly rotated CIFAR-10 images (i.e., in the range of $\pm 30^\circ$), similar to the setting of the first experiment. During testing, however, we supply each local client with 2000 test images subjected to related but completely unseen transformations (i.e., 90° and -90° rotations).

Our results are summarized in Table 2. First, we measure the performance of CA-FEDPNAS and FEDDSNAS without any weight retraining. When received no additional information from the unseen tasks, both methods perform poorly as expected. While CA-FEDPNAS achieves better predictive accuracy, the performance gap in this scenario is negligible. To provide additional clues for adaptation, albeit minimal, we retrain the weights of each local model with 200 images rotated according to respective unseen task description. Here, the parameters of our operator sampler component, (and respectively, FEDDSNAS’s categorical distribution parameters), are frozen to gauge the quality of the learned architecture distributions. Our results show that, with only 100 retraining iterations on limited data, CA-FEDPNAS already outperforms FEDDSNAS (5% and 8% improvement respectively on two unseen tasks). This implies that CA-FEDPNAS has more accurately capture the broad similarity of the task spectrum through the personalized architecture distribution, which requires minimal additional information to successfully adapt to unseen tasks.

5 Conclusion

We demonstrate that federated learning for multi-task scenarios requires extensive personalization on the architecture level to obtain good predictive performance. This paper identifies two potential sources of model personalization: (1) task-personalization, which aims to select architectures best suited for specific learning objectives; and (2) context-personalization, which aims to select architectures best suited for specific input samples. To incorporate these aspects of personalization into Federated NAS, we propose FEDPNAS which consists of two main components: (1) a context-aware operator sampler which learns a sampling distribution for feature maps along a master architecture; and (2) a personalized federated learning objective which anticipates client fine-tuning and guides the federated model update to regions that tolerate future local updates.

UNSEEN TASK DESCRIPTION	FEDDSNAS	CA-FEDPNAS	FEDDSNAS (RETRAINED)	CA-FEDPNAS (RETRAINED)
ROTATE -90	0.545 ± 0.04	0.578 ± 0.09	0.699 ± 0.12	0.734 ± 0.17
ROTATE 90	0.553 ± 0.12	0.569 ± 0.06	0.673 ± 0.13	0.727 ± 0.22

Table 2: Predictive accuracy (averaged over 5 clients) and standard deviation of CA-FEDPNAS and FEDDSNAS on two unseen tasks (CIFAR-10). The best performance in each row is in bold font.

6 Acknowledgement

This work was supported in part by the Gordon and Betty Moore Foundation’s Data-Driven Discovery Initiative [GBMF4554 to C.K.], the US National Institutes of Health [R01GM122935], and the US National Science Foundation [DBI-1937540]. Conflict of Interest: C.K. is a co-founder of Ocean Genomics, Inc.

References

- B. Baker, O. Gupta, N. Naik, and R. Raskar. Designing neural network architectures using reinforcement learning. *arXiv preprint arXiv:1611.02167*, 2016.
- J. Bergstra, D. Yamins, and D. Cox. Making a science of model search: Hyperparameter optimization in hundreds of dimensions for vision architectures. In *International Conference on Machine Learning*, pages 115–123. PMLR, 2013.
- A. Fallah, A. Mokhtari, and A. Ozdaglar. Personalized federated learning: Model-agnostic meta-learning approach. In *Proc. NeurIPS*, 2020.
- C. Finn, P. Abbeel, and S. Levine. Model-agnostic meta-learning for fast adaptation of deep networks. In *Proc. ICML*, pages 1126–1135, 2017.
- D. Floreano, P. Dürr, and C. Mattiussi. Neuroevolution: from architectures to learning. *Evolutionary Intelligence*, 1(1):47–62, 2008.
- C. He, M. Annavaram, and S. Avestimehr. Fednas: Federated deep learning via neural architecture search. *arXiv e-prints*, pages arXiv–2004, 2020.
- M. Hoang, N. Hoang, B. K. H. Low, and C. Kingsford. Collective model fusion for multiple black-box experts. In *International Conference on Machine Learning*, pages 2742–2750. PMLR, 2019a.
- N. Hoang, T. Lam, B. K. H. Low, and P. Jaillet. Learning task-agnostic embedding of multiple black-box experts for multi-task model fusion. In *International Conference on Machine Learning*, pages 4282–4292. PMLR, 2020.
- T. N. Hoang, Q. M. Hoang, K. H. Low, and J. P. How. Collective online learning of Gaussian processes in massive multi-agent systems. In *Proc. AAAI*, 2019b.
- J. Hu, L. Shen, and G. Sun. Squeeze-and-excitation networks. In *Proceedings of the IEEE Conference on Computer Vision and Pattern Recognition*, pages 7132–7141, 2018.
- S. Hu, S. Xie, H. Zheng, C. Liu, J. Shi, X. Liu, and D. Lin. DSNAS: Direct neural architecture search without parameter retraining. In *Proceedings of the IEEE/CVF Conference on Computer Vision and Pattern Recognition*, pages 12084–12092, 2020.
- E. Jang, S. Gu, and B. Poole. Categorical reparameterization with gumbel-softmax. *arXiv preprint arXiv:1611.01144*, 2016.
- D. M. Kane and J. Nelson. Sparser Johnson-Lindenstrauss transforms. *Journal of the ACM (JACM)*, 61(1):1–23, 2014.
- A. Krizhevsky et al. Learning multiple layers of features from tiny images. *Citeseer*, 2009.
- T. C. Lam, N. Hoang, B. K. H. Low, and P. Jaillet. Model fusion for personalized learning. In *International Conference on Machine Learning*, pages 5948–5958. PMLR, 2021.
- Y. LeCun, C. Cortes, and C. Burges. MNIST handwritten digit database. *ATT Labs [Online]*, 2, 2010. URL <http://yann.lecun.com/exdb/mnist>.
- T. Li, A. K. Sahu, A. Talwalkar, and V. Smith. Federated learning: Challenges, methods, and future directions. *IEEE Signal Processing Magazine*, 37(3):50–60, 2020.
- H. B. McMahan, E. Moore, D. Ramage, S. Hampson, and B. A. y Arcas. Communication-efficient learning of deep networks from decentralized data. In *Proc. AISTATS*, pages 1273–1282, 2017.

- H. Pham, M. Y. Guan, B. Zoph, Q. V. Le, and J. Dean. Efficient neural architecture search via parameter sharing. *arXiv preprint arXiv:1802.03268*, 2018.
- E. Real, A. Aggarwal, Y. Huang, and Q. V. Le. Regularized evolution for image classifier architecture search. In *Proceedings of the AAAI Conference on Artificial Intelligence*, volume 33, pages 4780–4789, 2019.
- T. V. Vo, T. N. Hoang, Y. Lee, and T.-Y. Leong. Federated estimation of causal effects from observational data. *arXiv preprint arXiv:2106.00456*, 2021.
- S. Xie, H. Zheng, C. Liu, and L. Lin. SNAS: stochastic neural architecture search. *arXiv preprint arXiv:1812.09926*, 2018.
- M. Yurochkin, M. Agarwal, S. Ghosh, K. Greenewald, and N. Hoang. Statistical model aggregation via parameter matching. *Advances in Neural Information Processing Systems*, 32:10956–10966, 2019.
- B. Zoph and Q. V. Le. Neural architecture search with reinforcement learning. *arXiv preprint arXiv:1611.01578*, 2016.

A FEDPNAS Algorithmic Details

Algorithm 1 FEDPNAS - FEDERATED PHASE

```

1: CENTRALAGGREGATION:
2:  $\theta_0 \leftarrow \text{INITIALIZEPARAMETER}$ 
3: for  $t = 1, 2 \dots T_s$  do
4:   for  $k = 1, 2 \dots M$  in parallel do
5:      $\theta_t^k \leftarrow \text{CLIENTUPDATE}(k, \theta_{t-1})$ 
6:    $\theta_t \leftarrow \sum_{k=1}^M \frac{1}{M} \theta_t^k$ 
7: CLIENTUPDATE( $k, \theta$ ):
8: for  $t = 1, 2 \dots T_c$  do
9:   for batch  $(x, y) \in \mathcal{D}_k$  do
10:     $\mathcal{L}_k, \nabla \mathcal{L}_k \leftarrow \text{EVAL}(x, y; \theta_b, \theta_p)$ 
11:     $\tilde{\theta}_p \leftarrow \text{GRADUPDATE}(\nabla_{\tilde{\theta}_p} \mathcal{L}_k)$ 
12:     $\tilde{\mathcal{L}}_k, \nabla \tilde{\mathcal{L}}_k \leftarrow \text{EVAL}(x, y; \theta_b, \tilde{\theta}_p)$ 
13:     $\nabla_{\theta_p} \tilde{\mathcal{L}}_k \leftarrow \text{EQ. 4}$ 
14:     $\theta_b, \theta_p \leftarrow \text{GRADUPDATE}(\nabla_{\theta_b, \theta_p} \tilde{\mathcal{L}}_k)$ 
15: return  $\theta$  to central server

```

Algorithm 2 FEDPNAS - EVAL

```

1: Input:  $x, y, \theta$ 
2: SKIP, PREV  $\leftarrow x, x$ 
3:  $\mathbf{W}, \mathbf{\Pi} \leftarrow \theta$ 
4: for CELL  $\psi \in \Psi$  do
5:    $\mathbf{Z} \leftarrow \text{SAMPLEOPS}(x, \text{PREV}; \mathbf{\Pi})$ 
6:    $\psi \leftarrow \text{EXTRACTCHILDNET}(\mathbf{Z}, \mathbf{W})$ 
7:   if  $\psi \in \Psi_b$  then
8:     OUTPUT  $\leftarrow \psi(\text{PREV}, \text{SKIP})$ 
9:   else if  $\psi \in \Psi_p$  then
10:    OUTPUT  $\leftarrow \psi(\text{PREV})$ 
11:    SKIP  $\leftarrow \text{PREV}$ 
12:    PREV  $\leftarrow \text{OUTPUT}$ 
13:    $\mathcal{L} \leftarrow \text{LOSS}(\text{OUTPUT}, y)$ 
14:    $\nabla \mathcal{L} \leftarrow \text{BACKPROP}(\mathcal{L})$ 
15: return  $\mathcal{L}, \nabla \mathcal{L}$ 

```

B Layer Operators

Table 3 below gives the list of operators available for sampling at every edge of the over-parameterized architecture search space. The implementation details of each operator type follows that of SNAS [Xie et al., 2018] and DSNAS [Hu et al., 2020]. Even though the master architecture has nearly a million parameters, we note that each learning batch only samples a fraction of these parameters to update.

Our implementation code is published at <https://github.com/hqminh/fedpnas>.

OPERATOR	FILTER SIZE	NO. PARAMS (CIFAR-10)	NO. PARAMS (MNIST)
AVGPOOL	3×3	64	32
MAXPOOL	3×3	64	32
SEP CONV	3×3	2752	864
SEP CONV	5×5	3776	1376
DIL CONV	3×3	1376	432
DIL CONV	5×5	1888	688
HOURLGLASS CONV	$7 \times 1, 1 \times 7$	14400	3616
SKIPCONNECT	N/A	0	0
MASTEREDGE		29632	9184
MASTERARCHITECTURE		948224	293888

Table 3: List of operators to be sampled from at every edge and their respective number of parameters in the CIFAR-10 experiment (32 channels) and the MNIST experiment (16 channels). MASTEREDGE denotes the combination of all operators at every edge in the network and MASTERARCHITECTURE denotes the combination of all operators in the network (total of 32 edges).

C Architecture for Federated Averaging

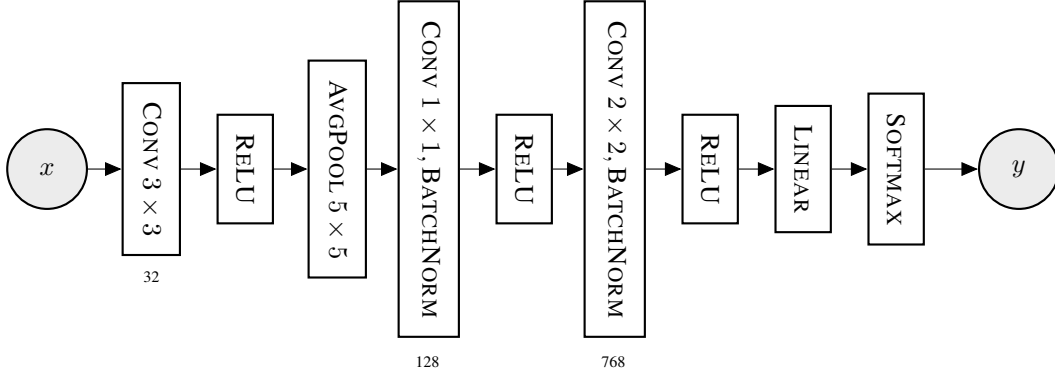


Figure 4: Architecture used for FEDAVERAGING method in our experiments (Section 4). The text below each CONV layer denotes the corresponding number of output channels. The expected number of input channels is 3. The final LINEAR layer flattens the channels and provides a mapping to an output dimension equals to the number of label classes (i.e. 10 for both CIFAR-10 and MNIST dataset).

D Theoretical connection to standard gradient update

Finally, we analyze the connection of our gradient update framework to the standard gradient update, and explain why it is critical in achieving a *vantage* point that improves average objective value without compromising any local objective. First, we note that the gradient update Eq. 4 in Section 3.2 at the t -th iteration can be written as:

$$\theta_p^{t+1} = \theta_p^t - \frac{\eta_2}{M} \sum_{i=1}^M \nabla_{\theta_p} \mathcal{L}_i(\theta_b^t, \tilde{\theta}_{p,i}^t) + \frac{\eta_1 \eta_2}{M} \sum_{i=1}^M \alpha_i \nabla_{\theta_p} \mathcal{L}_i(\theta_b^t, \theta_p^t),$$

$$\text{and } \theta_b^{t+1} = \theta_b^t - \frac{\eta_2}{M} \sum_{i=1}^M \nabla_{\theta_b} \mathcal{L}_i(\theta_b^t, \tilde{\theta}_{p,i}^t), \quad (5)$$

where $\tilde{\theta}_{p,i}^t$ denotes the i -th local personalized parameters; η_1 and η_2 are two separate learning rates and $\alpha_i \triangleq \nabla_{\theta_p}^\top \mathcal{L}(\theta_b^t, \theta_{p,i}^t) \nabla_{\theta_{p,i}} \mathcal{L}(\theta_b^t, \tilde{\theta}_{p,i}^t)$ (See Appendix A for detailed derivation). This implies that our federated personalized update corresponds to a federated update scheme with three gradient steps: (1) θ_p takes a *local* gradient (w.r.t. locally updated parameters) step of size η_1 ; (2)

Both θ_b and θ_p take a *federated* gradient (w.r.t. server-wide parameters averaging) step of size η_2 ; (3) θ_p takes a *weighted federated* gradient step of size $\eta_1 \eta_2$, where the weight of client i is given by α_i .

Explicitly, Step 1 and 2 together comprise a special instance of FEDAVERAGING [McMahan et al., 2017], where θ_b take one gradient step for every two gradient steps taken by θ_p . Step 3, on the other hand, takes the information of the two gradient steps of θ_p and adjust the magnitude of the local gradient step (whose direction is given by $\nabla_{\theta_p} \mathcal{L}_i(\theta_b^t, \theta_p^t)$) accordingly to trade-off between preserving local objective value and improving average objective value. We then theorize the scenario in which such an update is beneficial and state the following assumption to lay the foundation of our analysis:

Assumption 1 For a fixed instance of θ_b , let $\tilde{\theta}_{p,i} = \theta_{p,i} - \eta \nabla_{\theta_p} \mathcal{L}(\theta_b, \theta_{p,i})$ denote the personalized parameters after a local update step (i.e., step 1 above) at client i , then there exists a distribution \mathcal{S} on matrix $\mathbf{S} \in \mathbb{R}^{k \times |\theta_p|}$ that satisfies

$$\forall \mathbf{x} \in \mathbb{R}^n, \|\mathbf{x}\|_2 = 1 : \mathbb{E}_{\mathbf{S} \sim \mathcal{S}} [\|\mathbf{S}\mathbf{x}\|_2^2 - 1]^{\ell} \leq \epsilon^\ell \cdot \delta, \quad (6)$$

$$\Pr_{\mathbf{S} \in \mathcal{S}} \left(\left| \nabla_{\theta_p} \mathcal{L}(\theta_b, \tilde{\theta}_{p,i}) - \mathbf{S}^\top \mathbf{S} \left(\frac{1}{M} \sum_{i=1}^M \nabla_{\theta_p} \mathcal{L}(\theta_b, \tilde{\theta}_{p,i}) \right) \right| \leq \sqrt{\frac{6}{k\delta}} \right) \geq 1 - \delta, \quad (7)$$

where $k = \mathcal{O}(C \|\theta_b - \theta_b^*\|_2^{-2})$ for some constant $C > 0$ and θ_b^* denotes the optimal base parameters.

The above assumption implies that, as θ_b improves and better captures the broad similarity across tasks, the local personalized components will diverge to capture the differences. It then becomes less likely for the FEDAVG personalized gradient to capture all these differences simultaneously. That is, suppose there exists an affine transformation to reconstruct the local component $\nabla_{\theta_p} \mathcal{L}_i(\theta_b^t, \tilde{\theta}_p^t)$ from the federated gradient $\mathbf{L} \triangleq \frac{1}{M} \sum_{i=1}^M \nabla_{\theta_p} \mathcal{L}_i(\theta_b^t, \tilde{\theta}_p^t)$, then the rank of this affine transformation would be inversely proportionate to $\|\theta_b - \theta_b^*\|_2$.

Finally, Proposition 1 below shows that when this assumption holds and θ_b converges to the optimal parameter θ_b^* (i.e., the error term tends to 0), then with very high probability, the coefficient α_i of the *weighted* federated gradient step (i.e., step 3 above) accurately captures the cosine similarity between the local gradient (step 1) and the federated gradient (step 2).

Proposition 1 Suppose assumption 1 holds, then with probability at least $1 - 2\delta$ and normalized gradients, we have:

$$\left| \alpha_i - \nabla_{\theta_p}^\top \mathcal{L}_i(\theta_b^t, \theta_p^t) \mathbf{L} \right| = \mathcal{O}(\|\theta_b - \theta_b^*\|/\delta) \quad (8)$$

Proof. See Appendix B

This result has strong implication with respect to the scenario with multiple heterogeneous tasks, whose local gradients contradict in directions. Per this setting, we expect a standard federated gradient update scheme to encourage parameters drifting in the general direction of the majority (i.e., captured by the federated gradient), thus worsening the performance of tasks that are in the minority. Proposition 1, however, implies that whenever the local gradient contradicts the federated gradient, α_i will be close to the cosine similarity term, which is negative. This in turn results in a dampening effect on the federated gradient and helps to preserve the client performance on its own local task.

E Proof of Eq. 5

The update Eq. (4) in Section 3.2 for a single client at the t -th iteration can be written as:

$$\begin{aligned} \theta_p^{t+1} &= \theta_p^t - \eta_2 \left(\mathbf{I} - \eta_1 \nabla_{\theta_p} \mathcal{L}(\theta_b^t, \theta_p^t) \nabla_{\theta_p}^\top \mathcal{L}(\theta_b^t, \theta_p^t) \right) \nabla_{\theta_p} \mathcal{L}(\theta_b^t, \tilde{\theta}_p^t) \\ &= \theta_p^t - \eta_2 \nabla_{\theta_p} \mathcal{L}(\theta_b^t, \tilde{\theta}_p^t) + \eta_2 \eta_1 \nabla_{\theta_p} \mathcal{L}(\theta_b^t, \theta_p^t) \nabla_{\theta_p}^\top \mathcal{L}(\theta_b^t, \theta_p^t) \nabla_{\theta_p} \mathcal{L}(\theta_b^t, \tilde{\theta}_p^t) \\ &= \theta_p^t - \eta_2 \nabla_{\theta_p} \mathcal{L}(\theta_b^t, \tilde{\theta}_p^t) + \alpha \eta_1 \eta_2 \nabla_{\theta_p} \mathcal{L}(\theta_b^t, \theta_p^t), \\ \text{and } \theta_b^{t+1} &= \theta_b^t - \eta_2 \nabla_{\theta_b} \mathcal{L}(\theta_b^t, \tilde{\theta}_p^t), \end{aligned} \quad (9)$$

where η_1 and η_2 are two separate learning rates and $\alpha \triangleq \nabla_{\theta_p}^\top \mathcal{L}(\theta_b^t, \theta_p^t) \nabla_{\theta_p} \mathcal{L}(\theta_b^t, \tilde{\theta}_p^t)$. Factoring in the parameter averaging step in the federated phase, the overall update becomes³:

$$\begin{aligned} \theta_p^{t+1} &= \theta_p^t - \frac{\eta_2}{M} \sum_{i=1}^M \nabla_{\theta_p} \mathcal{L}_i(\theta_b^t, \tilde{\theta}_{p,i}^t) + \frac{\eta_1 \eta_2}{M} \sum_{i=1}^M \alpha_i \nabla_{\theta_p} \mathcal{L}_i(\theta_b^t, \theta_p^t), \\ \text{and } \theta_b^{t+1} &= \theta_b^t - \frac{\eta_2}{M} \sum_{i=1}^M \nabla_{\theta_b} \mathcal{L}_i(\theta_b^t, \tilde{\theta}_{p,i}^t), \end{aligned} \quad (10)$$

where α_i and $\tilde{\theta}_{p,i}^t$ are similarly defined with the local loss gradient of client i .

F Proof of Proposition 1

We have, with probability $1 - \delta$:

$$\begin{aligned} \left| \alpha_i - \nabla_{\theta_p}^\top \mathcal{L}_i(\theta_b^t, \theta_p^t) \mathbf{L} \right|^2 &= \left| \nabla_{\theta_p}^\top \mathcal{L}_i(\theta_b^t, \theta_p^t) \nabla_{\theta_p}^\top \mathcal{L}_i(\theta_b^t, \tilde{\theta}_p^t) - \nabla_{\theta_p}^\top \mathcal{L}_i(\theta_b^t, \theta_p^t) \mathbf{L} \right|^2 \\ &\leq \left| \nabla_{\theta_p}^\top \mathcal{L}_i(\theta_b^t, \theta_p^t) \mathbf{S}^\top \mathbf{S} \mathbf{L} + \sqrt{\frac{6}{k\delta}} - \nabla_{\theta_p}^\top \mathcal{L}_i(\theta_b^t, \theta_p^t) \mathbf{L} \right|^2 \end{aligned} \quad (11)$$

Since \mathcal{S} satisfies Eq. (8), we can apply the Approximate Matrix Product theorem [Kane and Nelson, 2014] with Union bound to obtain (with probability at least $1 - 2\delta$):

$$\begin{aligned} \left| \alpha_i - \nabla_{\theta_p}^\top \mathcal{L}_i(\theta_b^t, \theta_p^t) \mathbf{L} \right|^2 &\leq \frac{6}{k\delta} \left\| \nabla_{\theta_p}^\top \mathcal{L}_i(\theta_b^t, \theta_p^t) \right\|^2 \left\| \mathbf{L} \right\|^2 + \frac{6}{k\delta} \\ &\leq \frac{6}{k\delta} \frac{1}{M} \sum_{i=1}^M \left\| \nabla_{\theta_p}^\top \mathcal{L}_i(\theta_b^t, \tilde{\theta}_p^t) \right\|^2 + \frac{6}{k\delta} = \frac{12}{k\delta}, \end{aligned} \quad (12)$$

where the last inequality uses Cauchy-Schwartz inequality and the fact that all gradients are normalized since we only care about the direction of α_i in this analysis. Finally, by taking square root of both sides, this implies that with probability $1 - 2\delta$, we have: $\left| \alpha_i - \nabla_{\theta_p}^\top \mathcal{L}_i(\theta_b^t, \theta_p^t) \mathbf{L} \right| \leq \sqrt{\frac{12}{k\delta}} \simeq \mathcal{O}(\|\theta_b - \theta_b^*\|/\delta)$ by Assumption 1.

³Client indices are added when appropriate.